DIBR synthesized image quality assessment based on morphological wavelets

Conference Paper · May 2015

DOI: 10.1109/QoMEX.2015.7148143

CITATIONS
72

READS
219

3 authors:

Dragana D Sandić-Stanković
Institute for Telecommunications and Electronics IRITEL Beograd
44 PUBLICATIONS **258** CITATIONS
SEE PROFILE

Dragan Kukolj
RT-RK Computer Based Systems
125 PUBLICATIONS **1,187** CITATIONS
SEE PROFILE

Patrick Le Callet
University of Nantes
517 PUBLICATIONS **8,304** CITATIONS
SEE PROFILE

DIBR synthesized image quality assessment based on morphological wavelets

Dragana Sandić-Stanković
Institute for Telecommunication and Electronics IRITEL
Beograd, Serbia
dragana@iritel.com

Dragan Kukolj
Faculty of Technical Sciences
University of Novi Sad, Serbia
dragan.kukolj@rt-rk.com

Patrick Le Callet
IRCCyN Lab
Ecole polytechnique de l'Universite de Nantes, France
patrick.lecallet@univ-nantes.fr

***Abstract*—Most of the Depth Image Based Rendering (DIBR) techniques produce synthesized images which contain non-uniform geometric distortions affecting edges coherency. This type of distortions are challenging for common image quality metrics. Morphological filters maintain important geometric information such as edges across different resolution levels. In this paper, morphological wavelet peak signal-to-noise ratio measure, MW-PSNR, based on morphological wavelet decomposition is proposed to tackle the evaluation of DIBR synthesized images. It is shown that MW-PSNR achieves much higher correlation with human judgment compared to the state-of-the-art image quality measures in this context.**

Keywords— Multi-scale PSNR, morphological wavelets, nonseparable morphological wavelet decomposition, lifting scheme, quincunx sampling, DIBR synthesized image quality assessment

I. INTRODUCTION

Depth image-based rendering techniques can be used to generate views for free viewpoint television, 3DTV, 3D technology in entertainment, medical applications, etc. In all these use cases the success depends on the perceptual quality of synthesized views. Although much effort has been done in view modeling and synthesis, much less effort has been done on developing specific algorithms for assessing the visual quality of synthesized view. As the use of subjective tests is expensive, time consuming, cumbersome and cannot be implemented in the technical systems, the perceptual quality prediction of an images or video sequence is needed. DIBR algorithms introduce specific types of artifacts mostly located around disoccluded regions [1]. Typical rendering errors can include black hole, boundary blur, edge displacements or misalignments. These artifacts are consequently challenging for standard quality metrics, usually tuned for other type of distortions.

The evaluation of DIBR synthesized views from uncompressed data has been already discussed in literature for still images [1] and video [2]. It has been demonstrated that 2D quality metrics originally designed to address image and video compression distortions are very far to be effective to assess the visual quality of the synthesized image views.

Several metrics have been proposed to improve the performance obtained by standard quality metrics. The VSQA metric [3] is designed for artifacts detection in DIBR synthesized images and aimed to handle areas where disparity estimation may fail. It achieves the gain of 17.8% over SSIM in correlation to subjective measurements using IRCCyN/IVC DIBR image dataset [5]. 3DswIM metric [4] dedicated to artifact detection in DIBR-synthesized images relies on a comparison of statistical features of wavelet subbands of the original and DIBR-synthesized images. The 3DswIM metric achieves Pearson correlation of 76.17% on IRCCyN/IVC DIBR image dataset [5].

A. A novel multi-scale approach to tackle non-uniform geometric distortions

As in most other areas of image processing and analysis, multi-resolution methods have improved performances relative to single-resolution methods for image quality assessment. Multi-resolution decomposition using Haar wavelet is implemented as the first step of error-based image quality metrics [6]. Multiscale geometric analysis [7] uses a series of transforms including wavelet, curvelet, bandelet, contourlet, wavelet-based contourlet, hybrid wavelets and directional filter banks and then extract features to mimic the multichannel structure of human visual system. Multi-scale structural similarity measure, MS-SSIM [9] is based on linear low-pass pyramid decomposition. CW-SSIM is based on multi-orientation steerable pyramid decomposition using multi-scale bandpass oriented filters [10].

Multi-scale framework of image quality assessment can be seen as three-stage process. In the first stage both the reference and the distorted images are decomposed into a set of lower resolution images using multi-resolution decomposition. In the second stage image quality/distortion maps are evaluated at all

scales. In the third stage a pooling is employed to convert these maps into a single quality scores at all scales and finally these scores are combined into the multi-scale image quality measure.

In this paper, we propose morphological wavelet peak signal-to-noise ratio measure (MW-PSNR) based on morphological wavelet decomposition in order to better deal with specific geometric distortions in DIBR synthesized images. Introduced non-linear morphological filters maintain important geometric information such as edges across different resolution levels [11]. Both separable and nonseparable morphological wavelet decompositions are explored in the first stage of MW-PSNR. Also, we propose to calculate mean squared error (MSE) between the appropriate subbands of the wavelet representations of the reference and DIBR synthesized images. Multi-scale wavelet mean square error (MW-MSE) is calculated as the average MSE of all subbands and finally MW-PSNR is calculated from it. Since the morphological operators involve only integer, max, min and addition operations in their computation, the proposed metric MW-PSNR is of low computational complexity.

The next two sections introduce both separable and nonseparable morphological wavelet decompositions which will be explored in the first stage of MW-PSNR. Description of the distortion computation stage and pooling stage of the MW-PSNR measure is given in section IV. The performances of MW-PSNR and discussion are presented in section V, while the conclusion is given in section VI.

II. SEPARABLE MORPHOLOGICAL WAVELET DECOMPOSITION

Separable 2D morphological wavelet transforms are realized by cascading two 1D morphological wavelet transforms along the vertical and horizontal directions producing 3 detail subbands and approximation signal. After one scale of decomposition along each direction, the approximation subband is decomposed further, leading to the dyadic decomposition. In this paper, 1D morphological wavelet transformations, morphological Haar min wavelet and morphological min lifting wavelet, introduced in [14] and reviewed in [15] are explored for the MW-PSNR. 1D morphological wavelet transformations are implemented using the lifting scheme [12] using morphological operators in the prediction and update filtering step, Fig. 1.

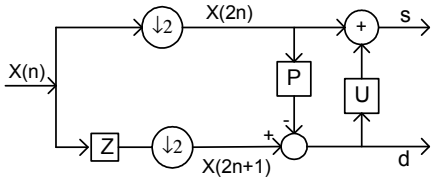

Fig. 1 – 1D DWT using the lifting scheme: prediction P and update U step; detail d and lower resolution signal s

A. 1D morphological Haar min wavelet transformation (minHaarWav)

One of the simplest example of non-linear morphological wavelets is the morphological Haar min wavelet. It is very similar structure to the linear Haar but it uses nonlinear operator erosion (minimum) in the update step of the lifting scheme. The pixel of the detail signal d and the pixel of the lower resolution signal s, are calculated from 2 samples, Fig.2:

$$d[n] = x[2n+1] - x[2n],$$
$$s[n] = x[2n] + \min(0, d[n]) \quad (1)$$

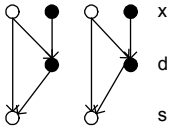

Fig.2. The calculation of the detail signal d and lower resolution signal s from higher resolution signal x using the lifting scheme for the linear Haar and the morphological Haar wavelet transform

For the comparision with linear case, 1D Haar wavelet transformation (HaarWav) is implemented using the lifting scheme. The detail signal d and lower resolution signal s (Fig.2) are calculated as:

$$d[n] = x[2n+1] - x[2n],$$
$$s[n] = x[2n] + \frac{1}{2} d[n] \quad (2)$$

The morphological Haar wavelet decomposition scheme may do a better job in preserving edges compared to linear case [14]. The signal analysis filters in the linear Haar wavelet decomposition scheme are linear lowpass filters and smooth-out edges while the signal analysis filters in the morphological Haar wavelet are nonlinear and preserve edges.

B. 1D morphological min lifting wavelet transformation (minLiftWav)

In the calculation of the morphological min lifting wavelet transform, the pixel of the detail d and the pixel of the approximation signal s are calculated using 3 samples, Fig. 3. Morphological operator erosion (minimum) is used in the predict and update step of the lifting scheme:

$$d[n] = x[2n+1] - \min(x[2n], x[2n+2])$$
$$s[n] = x[2n] + \min(0, d[n], d[n-1]) \quad (3)$$

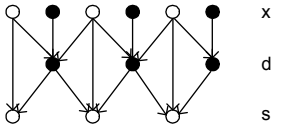

Fig.3. The calculation of the detail signal d and lower resolution signal s from higher resolution signal x using the lifting scheme for the morphological minLiftWav and cdf(2,2) wav.

For the comparision with linear case, biorthogonal (2,2) of Cohen-Daubechies-Feauveau wavelet (cdf(2,2)wav) using the lifting scheme [13] is implemented. The forward equations for the CDF(2,2) wavelet transform, Fig. 3, are:

$$d[n] = x[2n+1] - \frac{1}{2}(x[2n] + x[2n+2])$$
$$s[n] = x[2n] + \frac{1}{4}(d[n-1] + d[n]) \quad (4)$$

III. NONSEPARABLE MORPHOLOGICAL WAVELET DECOMPOSITION

Nonseparable sampling opens a possibility of having schemes better adapted to the human visual system [16]. Quincunx sampling is the simplest nonseparable multidimensional sampling structure. In the 2D separable wavelet decomposition, tensor product wavelet transform will favor horizontal, vertical and diagonal features of the image. Other features will not be easily detected. Nonseparable decomposition is expected to remove this drawback.

Nonseparable 2D wavelet transform on a quincunx lattice using the lifting scheme is performed through 2 steps, odd and even, producing 2 detail subbands and approximation signal. Each step, odd and even, consists of 3 parts: splitting, prediction and update. After one level of decomposition, the approximation subband is decomposed further. At first, in the odd step, the data are separated in two subsets, *x* and *y*, one with white pixels and the other with black pixels, Fig. 4a, both subsets on the quincunx lattice. Then the values of one subset (black pixels) are predicted from the other subset (white pixels) and the prediction error *d* is calculated, Fig. 4b. Next, the other dataset (white pixels) is updated with the errors (details) dataset to preserve the mean value of the data producing lower resolution signal *s*, Fig. 4c.

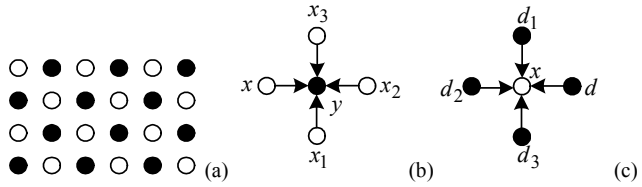

Fig. 4. The odd step of 2D non-separable decomposition on a quincunx lattice using the lifting scheme: a) quincunx sampling b) detail pixel *d* calculated in the prediction step c) lower resolution signal pixel *s* calculated in the update step

In the even step, the lower resolution signal pixels (white pixels) produced in the odd step are separated on two subsets, each on Cartesian lattice, one with white pixels and the other with gray pixels, Fig. 5a. The pixel of the error signal *d* is calculated from the 4 nearest pixels on diagonal directions, Fig. 5b and the lower resolution signal *s* is updated from 4 nearest detail signal pixels on diagonal directions, Fig. 5c.

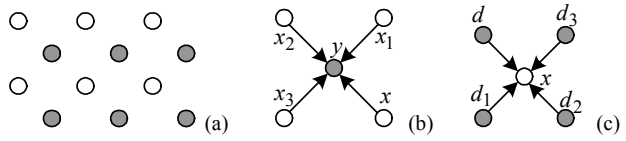

Fig. 5. The even step of 2D non-separable decomposition on a quincunx lattice using the lifting scheme: a) the signal in the quincinx lattice is split in two signals on Cartesian lattice b) the predict step c) the update step

A. Nonseparable morphological min lifting wavelet transformation with quincunx sampling (minLiftWavQ)

In this paper, nonseparable morphological wavelet decomposition on a quincunx lattice (minLiftWavQ) using the lifting scheme [18] is explored for the first stage of MW-PSNR. MinLiftWavQ wavelet of the nonseparable decomposition is analogue to the minLiftWav wavelet of the separable decomposition. The detail signal *d* and lower resolution signal *s* are calculated according to Fig. 4 in the odd step and according to Fig. 5 in the even step:

$$d = y - \min(x\ ,\ x_1,\ x_2,\ x_3)$$

$$s = x + \min(d,\ d_1,\ d_2,\ d_3, 0) \tag{5}$$

For the comparision with linear case, nonseparable 2D linear wavelet decomposition on a quincunx lattice (cdf(2,2)wavQ) using the lifting scheme [17] is explored. Linear wavelet cdf(2,2)wavQ of the nonseparable decomposition is analogue with the cdf(2,2)wav wavelet of the separable decomposition. The detail signal *d* and lower resolution signal *s* are calculated according to Fig. 4 in the odd step and according to Fig. 5 in the even step:

$$d = y - \frac{1}{4}(x + x_1 + x_2 + x_3)$$

$$s = x + \frac{1}{8}(d + d_1 + d_2 + d_3) \tag{6}$$

IV. DISTORTION COMPUTATION AND POOLING STAGE

Using wavelet transformation the image is decomposed into a large number of subbands. Since the human visual system is a complex system that is not completely known, properly combining the various subbbands into the final metric is difficult. Therefore, a simple approach achieving good accuracy is chosen. After the morphological wavelet decomposition of the reference and DIBR-synthesized images, squared error maps are calculated between the appropriate subbands of the two wavelet representation. From these maps, mean squared errors MSE_{ji} are calculated. Multi-scale wavelet mean squared error MW-MSE is calculated as weighted sum of MSE_{ji} values of all subbands at all scales of the two wavelet representations as final pooling,

$$MW-MSE = MSE_{M,D+1}\cdot\beta_{M,D+1} + \sum_{j=1}^{M}\sum_{i=1}^{D} MSE_{j,i}\cdot\beta_{j,i} \tag{7}$$

where equal value weights $\beta_{ji} = \frac{1}{M\cdot D+1}$ are used. M is the number of decomposition levels, D is the number of detail subbands at one decomposition level. In the case of separable wavelet transforms, D=3, while for the nonseparable wavelet decomposition, D=2. MSE_{ji} is the mean value of the squared error map of the subband *i* at decomposition level *j*:

$$MSE_{ji} = \frac{1}{N_{ji}\cdot K_{ji}} \sum_{k=1}^{K_j}\sum_{n=1}^{N_j} (x_{ji}(k,n) - y_{ji}(k,n))^2 \tag{8}$$

Finally, multi-scale morphological wavelet peak signal-to-noise-ratio MW-PSNR is calculated as:

$$MW-PSNR = 10\cdot\log_{10}\left(\frac{R^2}{MW-MSE}\right) \tag{9}$$

where R is the maximum dynamic range of the image.

V. RESULTS

We evaluate MW-PSNR performances using IRCCyN/IVC DIBR images database [5] introduced in [1]. It contains frames from 3 multi-view video sequences: Book Arrival (1024x768, 16 cameras with 6.5cm spacing), Lovebird1 (1024x768, 12 cameras with 3.5cm spacing), Newspaper (1024x768, 9 cameras with 5cm spacing). For each sequence four virtual views are generated on the positions corresponding to those positions obtained by the real cameras using seven depth image based rendering algorithms, named A1-A7 [19]–[24]. One key frame from each synthesized sequence is taken for the DIBR images database. For these key frames subjective assessment in form of mean opinion scores (MOS) is provided. The difference mean opinion scores (DMOS) is calculated as the difference between the reference frame's MOS and the synthesized frame's MOS.

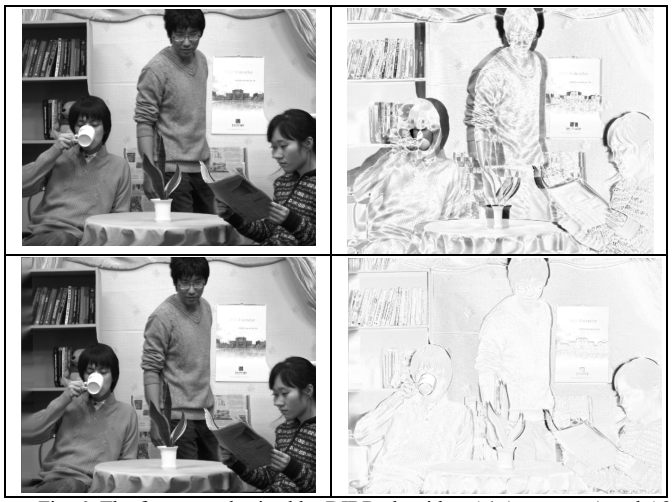

Fig. 6. The frame synthesized by DIBR algorithm A1 (upper row) and A2 (bottom row) and their inverted error maps.

The DIBR algorithms A1-A7 introduce artifacts mainly located around disoccluded areas. Typical DIBR artifacts are object shifting, geometric distortions, blurring, flickering. Object shifting artifact manifests as slight translation or resize of an image regions due to depth preprocessing including low-pass filtering. Blurry regions appear due to inpainting method used to fill the disoccluded areas. Incorrect rendering of textured areas appears when inpainting method fails in filling complex textured areas. Flickering appears when errors occur in depth data and pixels are wrongly projected. Geometric distortions include depth estimation errors, depth quantization errors in the conversion from depth data to depth map and inaccurate camera parameters. Although the shifting artifact exists in the frames synthesized using all A1-A7 algorithms, it is the most severe in the frames generated by algorithm A1 as it can be seen from Fig.6. The frames synthesized using algorithms A1 and A2 and corresponding error maps are shown on Fig. 6. The shifting artifact is significantly less noticeable using algorithm A2 than using A1. Therefore, the frames synthesized by algorithm A1 are excluded from the tests, so we focus on A2-A7 algorithms. Note that no registration procedure to align the synthesized and the original frames is applied.

To compare the performances of the image quality measures the following evaluation metrics are used: root mean squared error between the subjective and objective scores (RMSE), Pearson correlation coefficient with non-linear mapping between the subjective scores and objective measures (PCC) and Spearman's rank order correlation coefficient (SCC). The calculation of DMOS and non-linear mapping between the MOS and objective measures are done according to [25].

A. Performances of MW-PSNR

In this paper, the influence of different morphological wavelet decompositions on the MW-PSNR performances is explored. Separable morphological wavelet decompositions using minHaarWav and minLiftWav are explored. For the comparision with linear case, HaarWav and cdf(2,2)wav are explored also. Nonseparable morphological wavelet decomposition with quincunx sampling using minLiftWavQ is explored. For the comparision with linear case, cdf(2,2)wavQ is explored also.

TABLE I. PERFORMANCES OF PSNR CALCULATED FOR EACH SUBBAND PAIR OF SEPARABLE WAVELET DECOMPOSITION USING MINHAARWAV

level	*subb. idex*	*RMSE*	*PCC*	*SCC*
	11	0.5606	0.5768	0.4110
1	12	0.6096	0.4595	0.2389
	13	0.5496	0.5989	0.3285
	21	0.5682	0.5610	0.4259
2	22	0.5912	0.5079	0.3691
	23	0.5911	0.5082	0.3179
	31	0.5056	0.6762	0.5598
3	32	0.5256	0.6431	0.5112
	33	0.6041	0.4745	0.2801
	41	0.4044	0.8080	0.7333
4	42	0.4470	0.7588	0.6054
	43	0.4893	0.7013	0.5796
	51	0.3660	0.8459	**0.8088**
5	52	0.3651	0.8468	0.7831
	53	**0.3576**	**0.8535**	0.7831
	61	0.4079	0.8042	0.7684
6	62	0.4139	0.7977	0.7253
	63	0.4350	0.7735	0.7282
	71	0.4826	0.7111	0.7071
7	72	0.3947	0.8181	0.7618
	73	0.4484	0.7570	0.6967
	74	0.4947	0.6932	0.6106

At first, we calculated PSNR performances of wavelet subbands separately. The reference and the DIBR synthesized images are decomposed into a set of lower resolution images using morphological Haar min wavelet decomposition. The performances of PSNR are calculated between the appropriate subbands of the two wavelet representations. The performances of PSNR for all wavelet subbands in 7 decomposition levels are presented in Table I. The best PSNR performances are obtained for the subband with index 53.

The performances of PSNR by subbands are calculated using other wavelet decompositions also. For each wavelet decomposition, the subband with the best PSNR performances is shown on Table II. The best PSNR performances, PCC=0.887, SCC=0.828, are obtained for the subband with index 61 using wavelet decomposition with minLiftWav.

TABLE II. THE BEST PSNR PERFORMANCES BY SUBBANDS FOR EACH WAVELET DECOMPOSITION

wavelet	*subb.*	*RMSE*	*PCC*	*SCC*
minHaarWav	53	0.3576	0.8535	0.7831
HaarWav	61	0.3691	0.8431	0.7939
minLiftWav	**61**	**0.3167**	**0.8872**	**0.8281**
cdf(2,2)wav	61	0.3558	0.8551	0.7671
minLiftWavQ	52	0.3478	0.8621	0.7777
cdf(2,2)wavQ	52	0.4279	0.7818	0.6493

Based on the results from Table I, the performances of PSNR calculated between the subbands from levels 4-7 (with indices 41-74) are much better than the performances of PSNR calculated between subbands from levels 1-3 (with indices 11-33). Therefore, we propose the reduced version of MW-PSNR using only these subbands with better PSNR performances from the higher decomposition levels 4-7. The performances of the reduced version of MW-PSNR for different wavelet decompositions are presented in Table III. The best performances, Pearson 0.885 and Spearman 0.83, are obtained using separable morphological Haar min wavelet decomposition.

TABLE III. PERFORMANCES OF **REDUCED VERSION OF MW-PSNR** USING ONLY SUBBANDS FROM DECOMPOSITION LEVELS 4-7

decomp.	*wavelet*	*RMSE*	*PCC*	*SCC*
separable	**minHaarWav**	**0.3188**	**0.8855**	**0.8298**
	HaarWav	0.3935	0.8194	0.7695
	minLiftWav	0.3878	0.8251	0.6990
	cdf(2,2)wav	0.4735	0.7239	0.5958
non separable	minLiftWavQ	0.3599	0.8514	0.7641
	cdf(2,2)wavQ	0.4508	0.7541	0.6126

For the comparision with reduced version of MW-PSNR, the performances of full version of MW-PSNR using all wavelet subbands are calculated. Different number of decomposition levels, from 1 to 8 is tested. The best MW-PSNR performances are obtained using 7 decomposition levels. Separable wavelet transformations are performed in M=7 levels producing 22 subbands. Nonseparable wavelet transformations using quincunx sampling are performed also in M=7 levels producing 15 subbands. The performances of the full version of MW-PSNR using different wavelet decompositions are presented in Table IV. From the Tables III and IV, we can conclude that for each type of wavelet, the performances of reduced version of MW-PSNR are better than the performances of full version of MW-PSNR.

TABLE IV. PERFORMANCES OF FULL VERSION OF MW-PSNR USING ALL WAVELET SUBBANDS

decomp.	*wavelet*	*RMSE*	*PCC*	*SCC*
separable	minHaarWav	**0.3565**	**0.8545**	**0.7750**
	HaarWav	0.4435	0.7632	0.6491
	minLiftWav	0.4017	0.8108	0.6816
	cdf(2,2)wav	0.5009	0.6836	0.5450
nonseparable	minLiftWavQ	0.3922	0.8206	0.7382
	cdf(2,2)wavQ	0.4756	0.7210	0.5779

Based on the results from Table III and Table IV, it can be concluded that for the same type of decomposition (separable or nonseparable) and the corresponding type of wavelet, the performances of MW-PSNR using morphological wavelets are better than the performances of MW-PSNR using linear wavelets. More precisely, the performances of MW-PSNR using minHaarWav are better than the performances of MW-PSNR that uses HaarWav; the performances of MW-PSNR using minLiftWav are better than the performances of MW-PSNR using cdf(2,2)wav; the performances of MW-PSNR that uses nonseparable wavelet decomposition with quincunx sampling using minLiftWavQ are better than the performances of MW-PSNR that uses cdf(2,2)wavQ.

Also, based on the results from Table III and Table IV, it can be concluded that the performances of MW-PSNR are better when the nonseparable wavelet decomposition with quincunx sampling is used than when the separable wavelet decomposition using analogue wavelets is used. More precisely, the performances of MW-PSNR using minLiftWavQ are better than the performances of MW-PSNR using minLiftWav.

The performances of some commonly used metrics are presented in Table V. Structural similarity SSIM [8] is calculated between the original and DIBR synthesized images using the given code [26]. In the last row of Table V, the performances of the proposed reduced version of MW-PSNR using minHaarWav are added. The performances of MW-PSNR are much better than the performances of the commonly used 2D metrics.

TABLE V. PERFORMANCES OF COMMONLY USED 2D METRICS

	RMSE	*PCC*	*SCC*
PSNR	0.4525	0.7519	0.6766
SSIM [26]	0.5513	0.5956	0.4424
MS-SSIM [9]	0.5127	0.6649	0.5188
MW-PSNR	**0.3188**	**0.8855**	**0.8298**

B. Computational complexity

Since the morphological operations involve only integer, min and addition in their computation the calculation of morphological wavelet representation is of low computational complexity. The number of operations needed for the calculation of the wavelet decomposition of the image with

size *NK* with the maximum number of decomposition levels is shown in Table VI. Separable wavelet decompositions are computationally less expensive than nonseparable wavelet decompositions. Morphological Haar wavelet decomposition, which provides the best MW-PSNR performances, has the lowest computational complexity. The calculation of MSE is also of low complexity (1 subtraction, 1 multiplication and 1 addition per pixel) and the number of pixels in the wavelet image representation is *NK*.

TABLE VI. NUMBER OF OPERATIONS IN THE CALCULATION OF WAVELET DECOMPOSITION: S SUBTRACTION, C COMPARISION, A ADDITION, M MULTIPLICATION

decomp.	Wavelet	operations number
separable	minHaarWav	$(S+C+A)\cdot\frac{4}{3}NK$
	HaarWav	$(S+M+A)\cdot\frac{4}{3}NK$
	minLiftWav	$(3C+S+A)\cdot\frac{4}{3}NK$
	cdf(2,2)wav	$(3A+2M+S)\cdot\frac{4}{3}NK$
non separable	minLiftWavQ	$(7C+S+A)\cdot 2NK$
	cdf(2,2)wavQ	$(7A+2M+S)\cdot 2NK$

VI. CONCLUSION

We propose the morphological multi-scale wavelet peak signal-to-noise-ratio measure MW-PSNR for the evaluation of DIBR synthesized images. It shows high improvement of performances (e.g. 13.3% of correlation over PSNR). Reduced version of MW-PSNR based on morphological Haar min wavelet, shows high correlations with human judgment, (Pearson 0.885, Spearman 0.829). Since the morphological operators involve only integers and only min and addition in their computation, as well as simple calculation of MSE, the MW-PSNR is computationally efficient procedure. It provides reliable DIBR synthesized image quality assessment even without any parameter adaptation and a precise registration process in the image preprocessing stage.

VII. ACKNOWLEDGEMENTS

This work was partially supported by the Ministry of Education, Science and Technological Development of the Republic of Serbia under Grant TR-32034 and by the Secretary of Science and Technology Development of the Province of Vojvodina under Grant 114-451-1075/2014-03 and by Qualinet.

REFERENCES

[1] E. Bosc, R. Pepion, P. Le Callet, M. Koppel, P. Ndjiki-Nya, M. Pressigout and L.Morin "Towards a New Quality Metric for 3-D Synthesized View Assessment", *IEEE Journal on Selected Topics in Signal Processing*, Sept. 2011.

[2] E. Bosc, P. L. Callet, L. Morin and M. Pressigout, "Visual quality assessment of synthesized views in the context of 3DTV", 3D-TV system with Depth-Image-Based Rendering, C. Zhu, Y. Zhao, L. Yu, and M. Tanimoto, Springer, New York, pp 439-473, 2013.

[3] P. Conze, P. Robert, L. Morin, "Objective View Synthesis Quality Assessment", Proc. SPIE, Stereoscopic Displays and Applications, Febr. 2012.

[4] F.Battisti, E.Bosc, M.Carli, P. Le Callet, S.Perugia, "Objective image quality assessment of 3D synthesized views", Elsevier Signal Processing: Image Communication, vol.30, pp. 78-88, January 2015.

[5] ftp://ftp.ivc.polytech.univ-nantes.fr/IRCCyN_IVC_DIBR_Images

[6] S. Rezazadeh, S. Coulombe, "A novel wavelet domain error-based image quality metric with enhanced perceptual performance", Int. Journal of Computer and Electrical Engineering, vol.4, no.3, June 2012.

[7] X.Gao, W.Lu, D.Tao, X.Li, "Image Quality Assessment Based on Multiscale Geometric Analysis", IEEE Trans. on Image Processing, vol.18, no. 7, July 2009.

[8] Z. Wang, A. C. Bovik, H. R. Sheikh and E. Simoncelli, "Image Quality Assessment: From Error Visibility to Structural Similarity", IEEE Trans. On Image Processing, April 2004.

[9] Z. Wang, E. Simoncelli and A. C. Bovik, "Multi-scale structural similarity for image quality assessment", Asilomar Conference on Signals, Systems and Computers, 2003.

[10] Z. Wang, E.Simoncelli, "Translation insensitive image similarity in complex wavelet domain", ICASSP, 2005.

[11] P.Maragos, R.Schafer, "Morphological systems for multidimensional signal processing", Proceedings of the IEEE, April 1990.

[12] W. Sweldens, "The lifting scheme: A construction of second generation wavelets", SIAM J. Math. Anal., 27(2), 1997

[13] W. Sweldens, P. Schroder, "Wavelets in Computer Graphics", ACM SIGGRAPH Course Notes, 1996

[14] H. Heijmans, J. Goutsias, "Multiresolution signal decomposition schemes-Part2: Morphological wavelets," IEEE Trans. on Image Processing., vol. 9, Nov. 2000, pp. 1897–1913.

[15] D. Sandić-Stanković, "Morphological Wavelets for 3D Volume Image Decorrelation", International Conference on Digital Signal Processing *DSP*, Corfu, Jun 2011

[16] J. Kovačević, M. Vetterli, "Nonseparable Two- and Three-Dimensional Wavelets", IEEE Trans. on Signal Processing, vol. 43, No.5, May 1995.

[17] G. Uytterhoeven, A. Bultheel, "The Red-Black Wavelet Transform", Proc. of IEEE Benelux Signal Processing Symposium, 1997.

[18] H. Heijmans, J. Goutsias, "Morphological pyramids and wavelets based on the quincunx lattice", Mathematical morphology and its applications to image and signal processing, vol.18, pp. 273-281, 2000.

[19] C.Fehn, "Depth image based rendering (DIBR), compression and transmission for a new approach on 3D-TV", SPIE IS&T Electronic Imaging, 5291, 93, 2004.

[20] A.Telea, "An image inpainting technique based on the fast matching method", Journal of graphics, GPU and game tools, 9(1), 23-34, 2004.

[21] Y.Mori, N.Fukushima, T.Yendo, T.Fujii and M.Tanimoto, "View generation with 3D warping using depth information for FTV", Signal Processing: Image Communication, 24(1-2), 65-72, 2009.

[22] K.Muller, A.Smolic, K.Dix, P.Merkle, P.Kauff and T.Wiegand, "View synthesis for advanced 3D video systems", EURASIP Journal on image and video processing, 1-12, 2008.

[23] P.Ndjiki-Nya, P.Koppel, M.Doshkov, H.Lakshman, P.Merkle, K. Muller and T.Wiegand, "Depth image based rendering with advanced texture synthesis for 3D video", IEEE Int. Conf. on Multimedia&Expo, 2010.

[24] M.Koppel, P.Ndjiki-Nya, M.Doshkov, H.Lakshman, P.Merkle, K. Muller and T.Wiegand, "Temporally consistent handling of disocclusions with texture synthesis for depth-image-based rendering ", IEEE Int. Conf. on Image Processing, 2010.

[25] VQEG HDTV Group, "Test Plan for Evaluation of Video Quality Models for Use with High Definition TV Content", 2009.

[26] https://ece.uwaterloo.ca/~z70wang/research/ssim/ssim_inde